Journal of Power Sources 244 (2013) 586–591

Contents lists available at SciVerse ScienceDirect

Journal of Power Sources

journal homepage: www.elsevier.com/locate/jpowsour

Short communication

Synthesis and electrochemical properties of $LiFePO_4$-graphite nanofiber composites as cathode materials for lithium ion batteries

Van Hiep Nguyen, En Mei Jin, Hal-Bon Gu*

Department of Electrical Engineering, Chonnam National University, Gwangju 500-757, South Korea

HIGHLIGHTS

- ► $LiFePO_4$-Graphite nanofiber(GNF) successfully prepared by the hydrothermal method.
- ► The increase in electronic conductivity, and discharge capacity are determined.
- ► The electronic conductivity of $LiFePO_4$-GNF (7%) is 5.32×10^{-3} S cm.$^{-1}$
- ► $LiFePO_4$-GNF (7%) shows the best electrochemical performances.

ARTICLE INFO

Article history:
Received 30 October 2012
Received in revised form
20 December 2012
Accepted 5 January 2013
Available online 21 January 2013

Keywords:
Lithium ion battery
Lithium iron phosphate
Hydrothermal reaction
Graphite nanofibers-antler
Conductivity

ABSTRACT

In this paper, the influences of graphite nanofiber-antler (GNF) adding on $LiFePO_4$ are studied by X-ray diffraction (XRD), field emission-scanning electron microscopy (FE-SEM), transmission electron microscopy (TEM), cyclic voltammetry (CV), charge/discharge tests, and Ac impedance spectroscopy. In the results, the XRD patterns index to a single-phase material having an orthorhombic olivine-type structure with a space group of Pnma. The 7% GNF-added $LiFePO_4$ demonstrates a higher conductivity than the pure $LiFePO_4$ samples. The electronic conductivity of 7% GNF-added $LiFePO_4$ is 5.32×10^{-3} S cm^{-1}. The CV curves show that the 7% GNF-added $LiFePO_4$ has higher electrochemical reactivity for lithium insertion and extraction than the pure $LiFePO_4$ with the current is 1.65 mA and the voltage between redox peaks is 0.25 V. A discharge capacity of 131.5 mAh g^{-1} is achieved at a current density of 0.1 mA cm^{-2} with a slight decline during cycling.

1. Introduction

Recently, many efforts have been tried to adapt the need of source energy and to decrease environmental pollution. Among them, lithium ion batteries are being researched as the most promising material. Several materials under the development of their usage as cathodes in lithium ion batteries, especially lithium iron phosphate ($LiFePO_4$), have been researched a lot. An olivine-type structure like $LiFePO_4$ has attracted attention due to its high theoretical capacity (170 mAh g^{-1}), non-toxic, inexpensive, and high stability at a high temperature [1–3]. It is used in many fields such as portable devices, electric vehicles, and hybrid electric vehicles. However, it has a serious disadvantage, which is low intrinsic electronic conductivity. It does not only limit many applications of $LiFePO_4$ but also decrease the ability of insertion and extraction of lithium ion from the layers of $LiFePO_4$. Thus, many efforts have been made to solve this main problem by coating electronically conductive materials [4], doping with some elements [1], and modulating particle properties like size, texture, and phase distribution [5]. Among them, the coating of an electronically conductive material is a good problem-solving candidate. To implement it, various methods have been developed such as hydrothermal method [6], solid-state method [1], and sol–gel method [7]. In this study, we choose the hydrothermal method and ball-milling process to synthesize. GNF is chosen as an electronically conductive material. The conducting connections will be improved when GNFs are used in the cathode materials. Here we report the novel preparation of $LiFePO_4$-GNF composite cathode in order to improve electronic conducting and cycling performance.

2. Experimental

To begin with, the precursor materials like $LiOH \cdot H_2O$ (Aldrich Co. 99.95%), $FeSO_4 \cdot 7H_2O$ (Aldrich Co. >99%), H_3PO_4 (Aldrich Co. >99.999%), and ascorbic acid ($C_6H_8O_6$ Aldrich Co. >99%) were

* Corresponding author. Tel.: +82 62 530 0740; fax: +82 62 530 0077.
E-mail address: hbgu@chonnam.ac.kr (H.-B. Gu).

0378-7753/$ – see front matter © 2013 Elsevier B.V. All rights reserved.
http://dx.doi.org/10.1016/j.jpowsour.2013.01.073

prepared to synthesize $LiFePO_4$ through a hydrothermal method. Molar ratio of Li:Fe:P is 3:1:1. After $C_6H_8O_6$ has been added to the above solution, the mixture is heated at 170 °C for 12 h by Teflon obturation vessel (TAF-SR-50, TAIATSU TECHNO) that was sealed in a stainless steel autoclave. The obtained solution was filtered and washed many time with distilled water. In order to improve the electrochemical properties of $LiFePO_4$, different wt% GNF was added into the solution of *N*-methylpyrrolidone (NMP) and $LiFePO_4$; and the mixture was then milled at 300 rpm for 10 h by Planetary Mono Mill. The obtained powders were pelleted and further heated at 500 °C for 1 h in a tube furnace (J-FCA, JISICO) under N_2 atmosphere. After cooling down to the room temperature, the $LiFePO_4$-GNFs were ball-milled again at 300 rpm for 10 h. Finally, the mixtures were dried at 90 °C for 12 h.

The crystalline phases of $LiFePO_4$-GNF composites were identified with X-ray diffraction (XRD, Dmax/1200, Rigaku) with scanning steps of 0.02° over the range 10°∼50°. The morphology of the GNF-added $LiFePO_4$ composites was studied by transmission electron microscopy (TEM, JEM-2000TrX II, JED, Japan).

The composite electrodes were made from mixtures of $LiFePO_4$-GNF composites with a conductive material as carbon black (SP-270) and a binder as polyvinylidenefluoride (PVdF) in a wt % = 70:25:5. After being ball-milled, the slurry was coated onto aluminum foil and dried at 90 °C for 1 h. The electrodes were roll-pressed (0.6 m min^{-1}, 20 μm), cut into 2 × 2 cm^2 sections, and dried again at 110 °C for 24 h under vacuum. The beaker-type batteries were assembled in an argon-filled glove box using lithium as the anode and 1 M $LiPF_6$/EC-DMC (1:1) as the electrolyte, separator as Celgard#2500 membrane.

The morphology of $LiFePO_4$-GNF electrode films was observed with a Hitachi S-4700 field emission-scanning electron microscope (FE-SEM), which had an accelerating voltage of 15 kV. Cyclic voltammetry was carried out on an automatic charge/discharge equipment (WBCS3000, WonATech Co.) with the scan rate was 0.1 mV s^{-1}. The electrochemical impedance measurements were performed with an IM6 impedance measurement system. Ac voltage of 20 mV amplitude over the frequency range from 10 mHz to 2 MHz. The charge-discharge experiment was carried out with an instrument of WonATech (WBCS3000) system, the voltage range between 2.5 and 4.0 V at room temperature to investigate the charge/discharge behavior.

3. Results and discussion

The XRD patterns of $LiFePO_4$-GNF powders with different wt% GNF conductive additives are illustrated in Fig. 1. All the patterns indexed to a single-phase material having an orthorhombic olivine-type structure with a space group of Pnma. The cell parameters of samples can be seen in Table 1. The lattice parameters decrease slightly after adding GNF. And the XRD results show that the only observed phase is $LiFePO_4$. It demonstrates that the GNF added samples do not change the crystal structure of $LiFePO_4$ nanoparticles. Moreover, the crystallite size (D) of the sample is also calculated by the Scherrer's equation:

$$D = \frac{0.89\lambda}{B\cos\theta} \quad (1)$$

where B is the full-width at a half maximum and λ is X-ray radiation of a wavelength (1.54056 Å). In the results, the crystallite sizes decreased since GNF was added. The values of $LiFePO_4$ with 0%, 3%, 5%, 7% wt. GNF are 66 nm, 47.5 nm, 39.8 nm, and 36.6 nm, respectively. This work will tend to the decrease in particle sizes that has an important role in the insertion and de-insertion capability of lithium ion into the bulk of cathode materials.

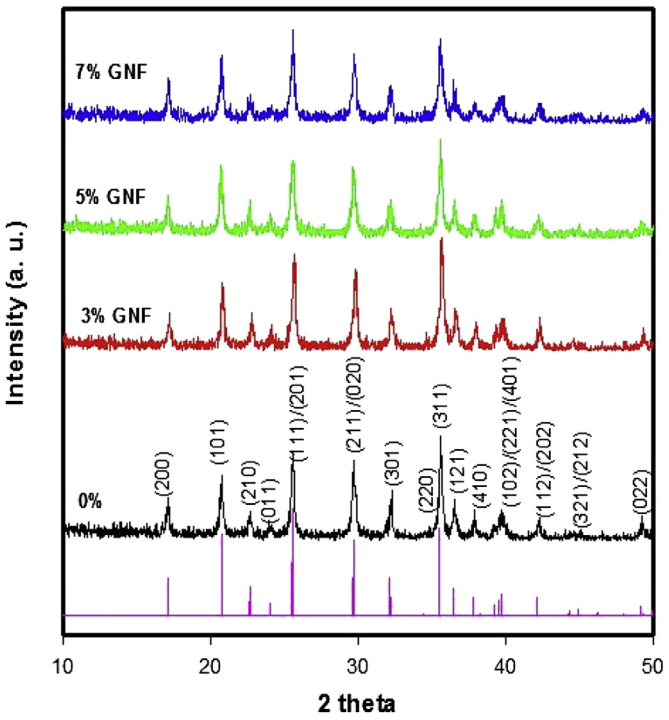

Fig. 1. XRD patterns for $LiFePO_4$- GNF composites.

In addition to intensity variation, the crystallizations of orientations and morphologies are calculated from Fig. 1. We can see the main trend in GNF-added patterns is gradually increased in intensity as compared to $LiFePO_4$ samples of the diffraction line, which may imply a preferential crystal growth of $LiFePO_4$ crystals under the present preparation conditions. In order to gain insights into the grain growth, the predominant crystallographic orientation of the crystals was determined from the XRD patterns by normalizing the measured diffraction intensities with the standard diffraction intensities for randomly oriented $LiFePO_4$ powders [8,9]. Herein, we attribute that a $LiFePO_4$ sample is the randomly oriented $LiFePO_4$ powder. The percentage of $LiFePO_4$-GNF crystals in different orientations (hkl) is estimated as following:

$$\%hkl = \frac{I_{hkl}/I^*_{hkl}}{\Sigma(I_{hkl}/I^*_{hkl})} \quad (2)$$

where I_{hkl} is the measured diffraction intensity of XRD peaks for $LiFePO_4$-GNF with 3%, 5%, 7%wt GNF and I^*_{hkl} is the diffraction intensity of XRD profile for $LiFePO_4$ powder. The calculation results are listed in Table 2. It is clearly observed that the percentages in orientations (210) for the GNF-added samples are obviously larger than those for the $LiFePO_4$ powder, which indicates the predominant nucleation planes (210).

The surface morphologies of the $LiFePO_4$-GNF films are determined by FE-SEM images in Fig. 2. In this figure, GNF was utilized as

Table 1
The unit cell parameters of $LiFePO_4$-GNF.

%GNF	a (Å)	b (Å)	c (Å)	V(Å^3)	Crystallite size (nm)
0%	10.3494	6.0359	4.6999	293.5949	66
3%	10.3622	5.9985	4.7089	292.6953	47.5
5%	10.3626	5.9726	4.7039	291.1326	39.8
7%	10.2938	5.9808	4.6930	288.9281	36.6

Table 2
Crystallographic orientation of $LiFePO_4$-GNF composites.

hkl	Standard intensity I^*_{hkl} (0%)	%*hkl* (3%GNF)	%*hkl* (5%GNF)	%*hkl* (7%GNF)
200	92	6.55	7.61	9.98
101	150	7.94	9.11	9.66
210	61	10.11	10.94	10.13
011	211	8.19	7.05	9.63
201	194	7.28	6.88	7.69
211	122	5.76	5.60	6.08
301	254	7.65	7.44	6.75
311	97	6.58	6.22	8.83
121	69	6.13	5.83	5.50
410	70	7.38	9.77	7.95
401	52	10.48	7.89	7.30
022	20	9.32	10.46	5.30

a transport infrastructure road between $LiFePO_4$ particles. TEM images of $LiFePO_4$-GNF are also estimated (see Fig. 3). Indeed, the appearance of GNF between $LiFePO_4$ particles is easily obtained from Fig. 3. Usually, Li^+ ions move around a particle and then come to the others. It takes a long way to transfer Li^+ ions. But by the appearance of GNF, Li^+ ions can move from this particle to the others more easily. The appearance of GNF enhances the connection availability between particles of $LiFePO_4$. Thus, lithium ions can diffuse between the particles more easily and the electrochemical properties of Li/$LiFePO_4$-GNF batteries will increase, especially in the electronic conductivity of $LiFePO_4$-GNF. In order to prove my above prediction and make it more clearly, the electronic conductivity of $LiFePO_4$-GNF is measured. In the results, electronic conductivities of $LiFePO_4$-GNFs are obviously improved from 1.09×10^{-9} S cm^{-1} of pure $LiFePO_4$ to 3.72×10^{-4} S cm^{-1}, 2.57×10^{-3} S cm^{-1}, 5.32×10^{-3} S cm^{-1} of $LiFePO_4$ with 3 wt%, 5 wt %, 7 wt% GNF, respectively.

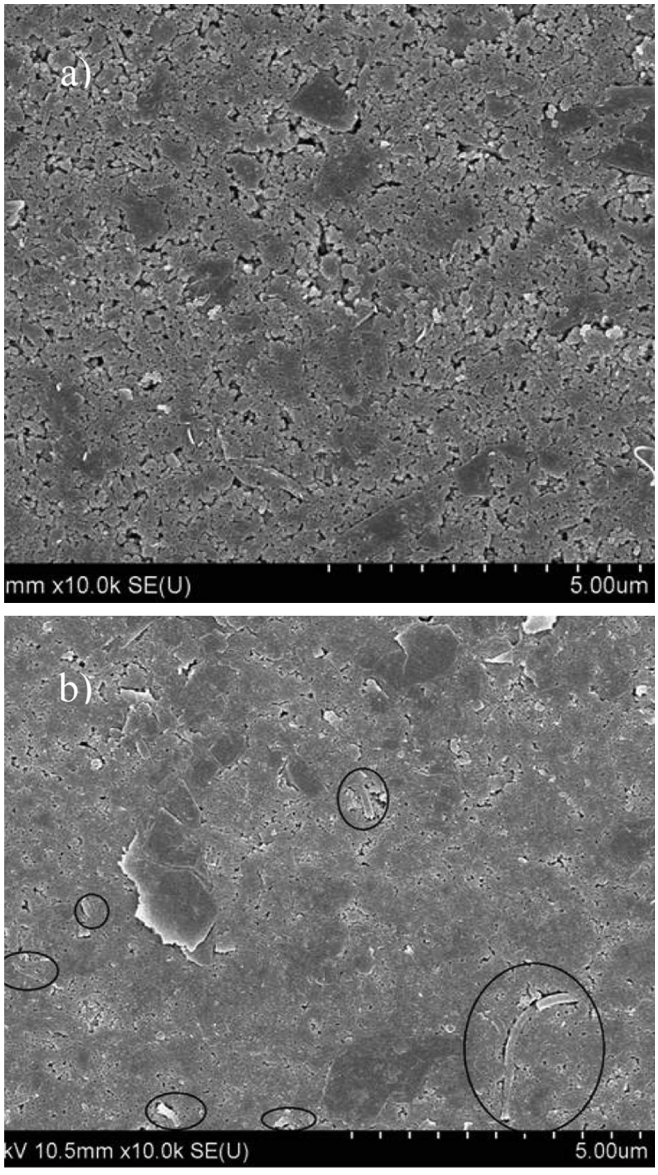

Fig. 2. FE-SEM images of $LiFePO_4$-GNF electrodes.

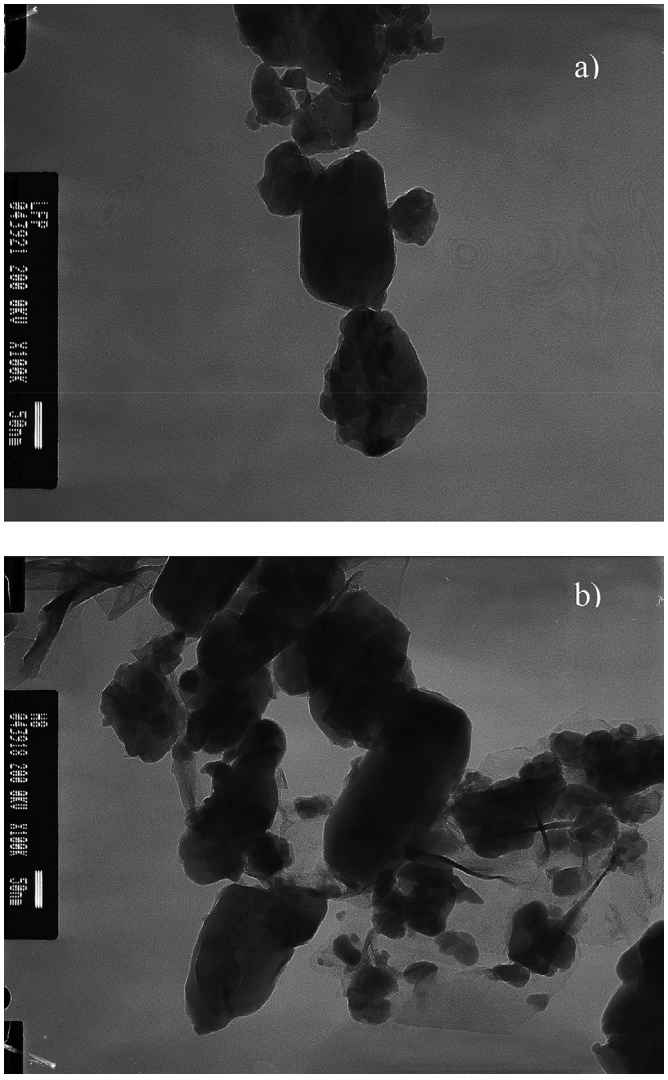

Fig. 3. TEM images of $LiFePO_4$-GNF powder: a) $LiFePO_4$, b) $LiFePO_4$-GNF.

The cyclic voltammograms of Li/$LiFePO_4$-GNF batteries with different wt% GNF conductive additives at the 3rd cycle are indicated in Fig. 4. We also recognize the fact that all oxidation and reduction peaks in the 3rd cycle appear at around 3.59 V and 3.28 V. The voltage between the oxidation and reduction peaks of pure Li/$LiFePO_4$ battery is 0.33 V. After adding GNF, there is a gradual decrease in the potential of the reduction peak and a slight increase in the potential of the oxidation peak. The differences from the potential of Li/$LiFePO_4$ with 3%, 5%, 7% GNF are 0.26 V, 0.27 V, and 0.25 V, respectively. Fig. 4 on the other hand shows that the current also increased significantly and the current of Li/$LiFePO_4$-GNF

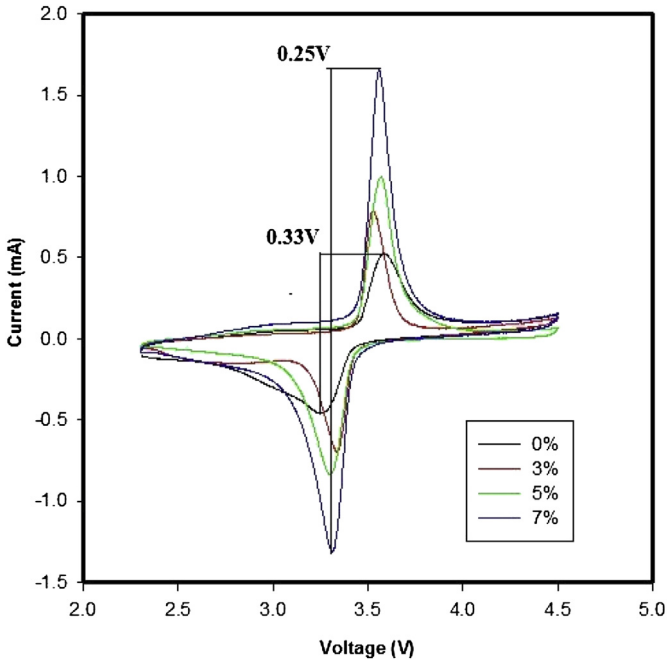

Fig. 4. Cyclic voltammograms of Li/$LiFePO_4$-GNF batteries at the 3rd cycle.

battery with 7% GNF shows the best value of 1.65 mA (meanwhile, 0.5 mA for pure $LiFePO_4$). These behaviors tend to suggest that by adding GNF, the charge-transfer kinetics is enhanced, that is consistent with our electrochemical system.

The reversibility of the Li/$LiFePO_4$-GNF batteries system is studied by varying the scan rate between 0.05 and 0.5 mV s^{-1}. These obtained results can be seen from CV profiles with different scan rate (see Fig. 5). As being obtained from Fig. 5, peak separation increases when increasing the scan rate. The oxidation peak and reduction peaks are highly symmetric to each other. The ratios of I_{pc}/I_{pa} are close to 1, which means that GNF-added $LiFePO_4$ has a good reversibility of lithium intercalation and de-intercalation.

The impedance spectra of Li/$LiFePO_4$-GNF batteries with different wt% GNF at the 3rd cycle are shown in Fig. 6. The frequency was scanned from high to low values in a range from 2 MHz to 10 mHz. The semicircles in the high to medium frequency are mainly related to a complex reaction process at the electrolyte/cathode interface. The inclined line in the lower frequency is attributed to the Warburg impedance, which is associated with lithium-ion diffusion in $LiFePO_4$ electrode. The impedance spectra can be interpreted on the basis of an equivalent circuit in which Z_w is Warburg impedance, R_{ct} is charge-transfer resistance, C_d is capacitance of a double layer, and R_s is ohmic resistance is shown in Fig. 6. The lithium ion diffusion coefficient is calculated by the following equation [10–13]:

$$D = \frac{R^2T^2}{2A^2n^4F^4C^2\sigma^2} \tag{3}$$

Herein n is the number of electrons per molecule during the oxidization, A is the surface area of the cathode, D is the diffusion coefficient of lithium ion, R is the gas constant (8.3144621 J mol^{-1}.K), T is the absolute temperature, F is the Faraday constant (96,485 J), C is the concentration of lithium ion [14], and σ is the Warburg factor which is interdependent on Z':

$$Z' = R_s + R_{ct} + \sigma\omega^{-1/2} \tag{4}$$

The interdependence between Z' and root square angular frequency $\omega^{-1/2}$ in the low frequency region is illustrated in Fig. 7.

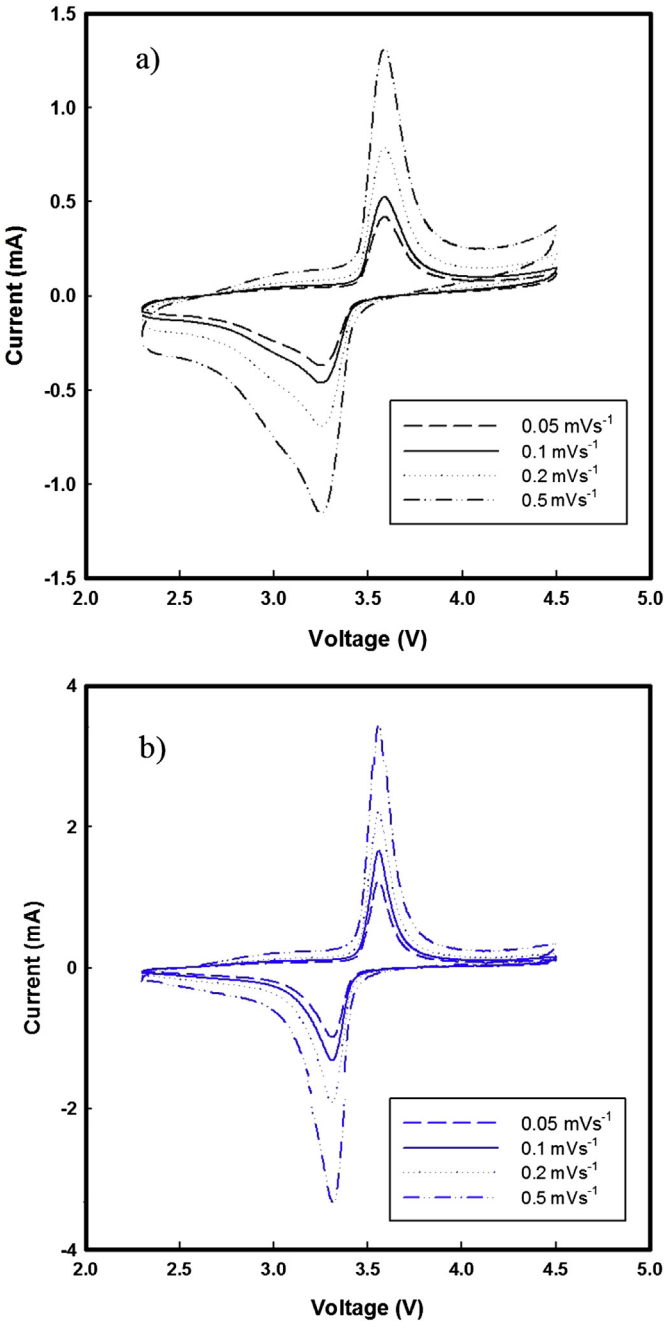

Fig. 5. Cyclic voltammograms profiles of Li/$LiFePO_4$-GNF batteries with different scan rates: a) 0%, b) 7% GNF.

Straight lines imply to the diffusion of the lithium ions into the layers of materials in the electrode materials. Furthermore, the exchange current density is calculated by the below equation:

$$i^o = \frac{RT}{nFR_{ct}} \tag{5}$$

The lithium ion diffusion coefficient is calculated from the equations (3)–(5) [15] and demonstrated in Fig. 7. All the results are pointed out in Table 3. It is clear from the data that both the lithium ion diffusion coefficient and the exchange current density increased. This is followed by the modest decline in the charge–discharge transfer. In the results, the lithium ion diffusion coefficient was improved to 2.23×10^{-14} cm^2 s^{-1}, the exchange current

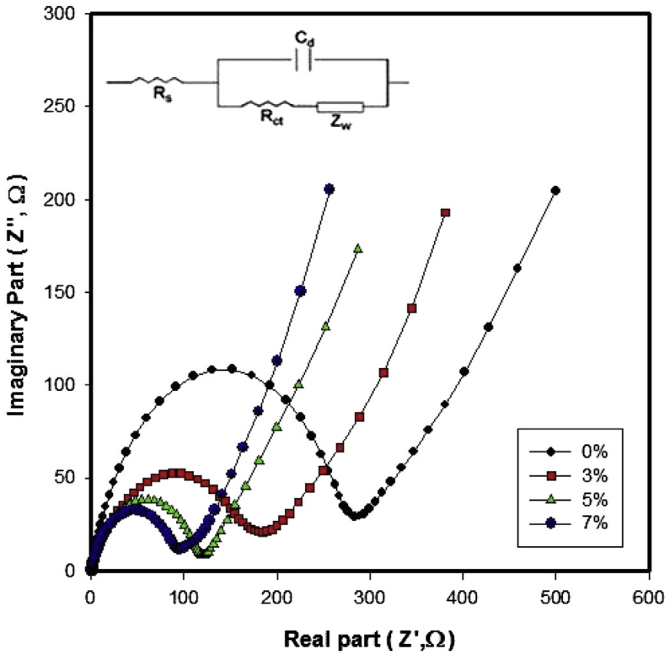

Fig. 6. Impedance spectra of Li/$LiFePO_4$-GNF batteries at the 3rd cycle.

density rose to 3.06×10^{-4} mA cm^{-2}, and the resistance decreased from 283 Ω to 84 Ω. This is in accordance with the CV results.

Fig. 8 illustrates the cycling performance of Li/$LiFePO_4$-GNF batteries that were charged–discharged at 0.1 mA cm^{-2} between 2.5 and 4.0 V. The discharge capacities of Li/$LiFePO_4$ battery appearing at the 2nd and 50th cycle are 113.8 mAh g^{-1} and 108.8 mAh g^{-1}, respectively. When adding wt. % GNF, the discharge capacity of the battery is increased. In correspondence with previous results such as XRD patterns, electronic conductivities, and FE-SEM, the insertion and de-insertion of lithium ions into the active material in the GNF-added $LiFePO_4$ electrode take place easily during the charging–discharging process. The Li/$LiFePO_4$-GNF battery with 7% GNF shows the best discharge capacity with a value of 131.5 mAh g^{-1} at the initial cycle and 99.8 mAh g^{-1} after 50 cycles. In comparison with Li/$LiFePO_4$ battery, the best discharge capacity of Li/$LiFePO_4$-GNF battery with 7% GNF increased by 15.8%. Therefore, 7% GNF addition is considered as the optimum concentration in this work. But the cycling stability and discharge capacity of composites in this work is too poor to compare to that of $LiFePO_4$ reported in many previous papers. This work can be explained that diameter of GNF and particle size of $LiFePO_4$ is not optimized completely so that the connection between $LiFePO_4$ particles is not good. We will improve this demerit in later study.

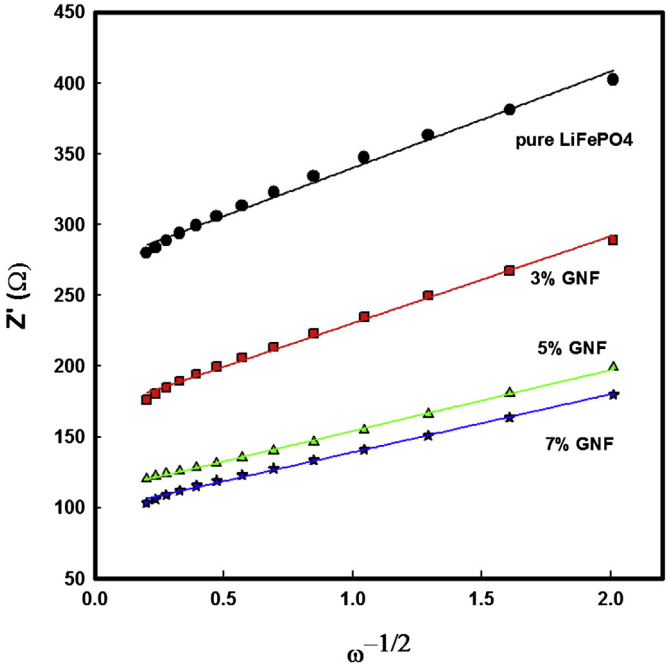

Fig. 7. The relationship between Z' and $\omega^{-1/2}$ in the low frequency range.

Table 3
Impedance parameters of the cells prepared from $LiFePO_4$-GNF composites.

%GNF	R_s (Ω)	R_{ct} (Ω)	D (cm^2 s^{-1})	i^o (mA cm^{-2})
0	0.8	283	8.09×10^{-15}	9.07×10^{-5}
3	0.8	185	1.01×10^{-14}	1.39×10^{-4}
5	0.8	118	2.02×10^{-14}	2.18×10^{-4}
7	0.8	84	2.23×10^{-14}	3.06×10^{-4}

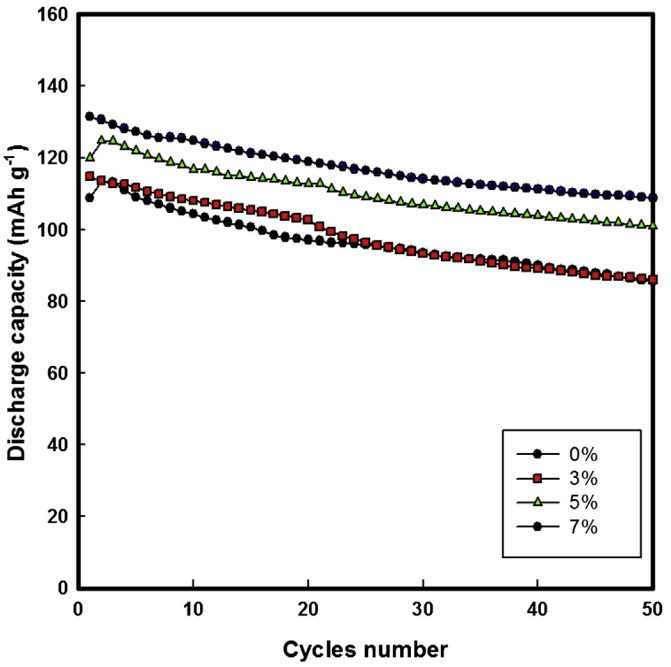

Fig. 8. Cycling performances of Li/$LiFePO_4$-GNF batteries.

4. Conclusions

After discussing all the points mentioned above, I can finally conclude that $LiFePO_4$-GNF composites have been synthesized successfully by the hydrothermal method and the subsequent ball-milling process. To improve the low electronic conductivity of $LiFePO_4$, different GNF additives were added. The XRD results demonstrated that $LiFePO_4$-GNF composites have an orthorhombic olivine-type structure with a space group of Pnma. The electronic conductivity of 7% GNF-added $LiFePO_4$ improved to 5.32×10^{-3} S cm^{-1}. At the meanwhile, the current reduction is 1.65 mA and the voltage between redox peaks is 0.25 V. The discharge capacity increases to 131.5 mAh g^{-1} at the current density of 0.1 mA cm^{-2}.

Acknowledgments

This research project received supporting funds from the second-stage Brain Korea 21.

References

[1] S.Y. Chung, J.T. Bloking, Y.M. Chiang, Nat. Mater. 1 (2002) 123–128.
[2] N.J. Yun, H.-W. Ha, K.H. Jeong, H.-Y. Park, K. Kim, J. Power Sources 160 (2006) 1361–1368.
[3] Bo Jin, H.-B. Gu, K.-W. Kim, J. Solid State Electrochem. 12 (2008) 105–111.
[4] S.T. Myung, S. Komaba, N. Hirosaki, H. Yashiro, N. Kumagai, Electrochim. Acta 49 (2004) 4213–4222.
[5] A. Yamada, S.C. Chung, K. Hinikuma, J. Electrochem. Soc. 148 (2001) A224.
[6] D.W. Choi, P.N. Kumta, J. Power Sources 163 (2007) 1064–1069.
[7] S. Franger, F.L. Cras, C. Bourbon, H. Rouault, J. Power Sources 119–121 (2005) 252–257.
[8] C. Damle, A. Kumar, S.R. Sainkar, M. Bhagawat, M. Sastry, Langmuir 18 (2002) 6075–6080.
[9] F. Zheng-Wei, G. Xiang-Feng, L. Li-Ping, L. Guang-She, Z. Jing, Chin. J. Struct. Chem. 30 (2011) 975–986.
[10] J.W. Yao, F. Wu, X.P. Qiu, N. Li, Y.F. Su, Electrochim. Acta 56 (2011) 5587–5592.
[11] C.K. Park, S.B. Park, S.H. Oh, H. Jang, W.I. Cho, Bull. Korean Chem. Soc. 32 (2011) 836–840.
[12] Atef Y. Shenouda, Hua K. Liu, J. Alloys Compd. 447 (2009) 498–503.
[13] X.H. Rui, N. Ding, J. Liu, C. Li, C.H. Chen, J. Electrochem. Acta 55 (2010) 2384–2390.
[14] A.J. Bard, L.R. Faulkner, Electrochemial Methods, second ed., Wiley& Sons, New York, 2001, p. 213.
[15] G.X. Wang, S. Bewlay, J. Yao, J.H. Ahn, S.X. Dou, H.K. Liu, Electrochem. Solid State Lett. 7 (2004) A503.